Laboratory of Nanoscience for Energy Technologies
Swiss Federal Laboratories for Materials Science and Technology

---

Report on the use of titanium nitride (20nm) provided by PlasmaChem: Photothermal conversion in TiN based nanofluids.

Supervisor:
Prof. Giulia Tagliabue

Co-Supervisor:
Dr. Artur Braun

Author:
Matteo Bevione

Abstract

Energy harvesting represents a promising tool to partially limit the wasted energy and consequently its production. The possibility to recover small quantities of power from the environment opens the door to self-supplied power devices, like wearable sensors or inaccessible remotely controlled systems. The sources to address for this purpose are electromagnetic radiation and wasted heat, thanks to their ubiquity and abundance. However, the low quality of the energy carried makes the currently available technology not efficient for its conversion, leading the researcher to explore new routes. Particularly interesting are the soft-robot application, which would be use in spatial exploration or rescue missions. This require a further degree of freedom, i.e. the high deformability of the system. For this reason, liquids and in particular nanofluids, results to be of interest. The purpose of COgITOR project is to realize a first prototype completely self-supplied, able to perform some basic computation and store information in liquid phase, leading the robot to acquire consciousness of the environment. In this work, preliminary studies are reported to address the problem of energy supply in liquid phase, by a photo-to-thermoelectric approach. The idea is to generate a stable temperature gradient inside a oil-based nanofluid to successively exploit the thermoelectric effect to supply energy to the robot. In this first part, titanium nitride is used as solid phase, thanks to its plasmonic properties providing an efficient photothermal conversion. Different light source are used to study the radiation dependence of this phenomena, and up to 93% conversion efficiency is reached. This result is in line with current literature and lay the foundation for the next step of conversion for sensor supply.

Keywords: Photothermal conversion, Alternative plasmonic materials, Titanium nitride, Energy Harvesting, Nanofluids.

1 Experimental Setup

1.1 Experimental Setups

In order to evaluate the possibility of establishing a stable temperature gradient inside the nanofluids, it is necessary to monitor the temperature throughout the fluid. However, it is difficult to find a commercial setup to accomplish this specific task. Thus, 3D printing is the preferred method to have a reproducible, easy and fast to realize (tens of hours) setup. Here the custom, in-house printed apparatus for photo-thermal characterization are reported. These have been realize in poly-lactic acid (PLA) with a fused deposition modeling (FDM) approach. SolidWorks® and CraftWare Pro Slicer software are used for design and slicing, respectively. The rationale behind realization of a custom setup lies in the ease of component modification. This gives freedom when it comes to investigation of the photothermal dependence on parameter like fluid volume, illuminated area and fluid volume.

1.1.1 Setup 1

This first setup, here reported in Fig. 1a is realized to provide optical alignment with the light source, i.e. the solar simulator or LEDs, for the testing in standard illumination conditions and radiation energy dependence. To prevent hating of the fluid container, referred as chamber hereinafter, a hemispherical slit or shutter is designed. This prevents the radiation to illuminate the structure limiting the active area to the fluid only. The lid of the chamber is equipped with six thermocouples evenly placed 5mm apart from each other. The chamber sizes are 20x20x40mm. A schematic view is also reported in 1b for a better comprehension of the system.

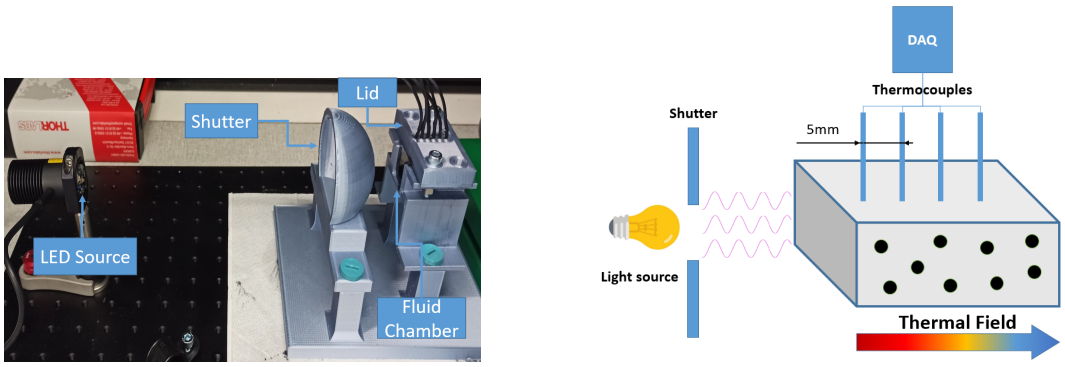

(*a*) (*b*)

Figure 1: *1a Real and 1b Schematic representation of the xperimental setup realized by Fused Deposition Modeling (FDM) in PLA.*

1.1.2 Setup 2

The Setup 1 accomplishes the job but is massive and takes a long time to print it. Moreover, its manipulation is not very simple. For this reason, the design is modified for two purposes: compactness, to achieve a faster print and an easier manipulation, and versatility, thanks to the realization of a further lid to host electrodes, needed for electrical characterization, also in view of investigation of thermoelectric nanofluids. The Setup 2, reported in Fig. 2a, has chamber dimensions of 10x10x25mm, equipped with a lid (see Fig. 2b) hosting eight type k thermocouples equally spaced by 2.5mm. A scheme is not reported since would be identical to 1b.

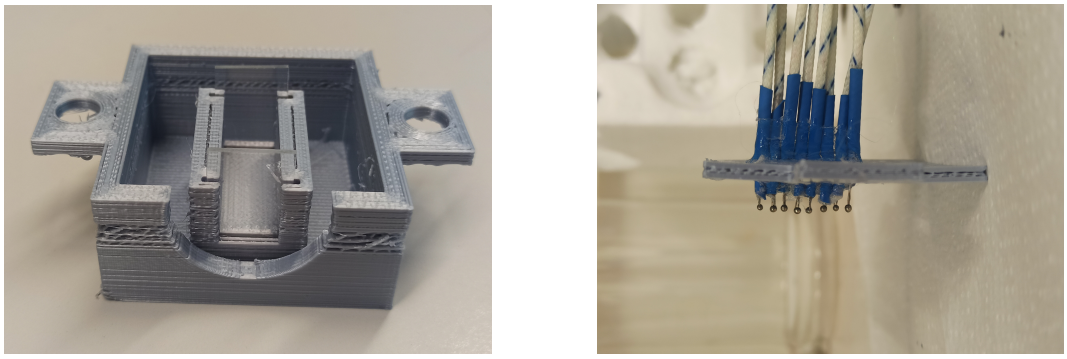

(*a*) (*b*)

Figure 2: *2a Compact experimental container for the nanofluid equipped with a shutter and 2b lid hosting type k thermocouples, realized by Fused Deposition Modeling (FDM) in PLA.*

1.2 Materials

As reported in previous sections, the material choice is extremely important depending upon the effect we want to observe. To clarify this, here the idea is to investigate the possibility to boost the thermoelectric effect occurring in some nanofluid, like graphene-oxide based colloids. [1] According to the literature, the electricity production in this kind of fluids occur mainly because of the movement of the electrical double layer (EDL) generated at the NP/solvent interface. [2] This net motion takes place because of the net force developed on the nanoparticles thanks to the temperature gradient. In other words, in a nanofluid the thermal diffusion of the solid fraction is faster than the solvent one, resulting in an accumulation of particles on the cold side. When a temperature gradient is built up, the particles start developing the EDL and migrating leading to a central region where the charge are compensated, neutral, while at the sides, a net voltage difference is built up. In the work of Anu *et al.*, [3] which have experimentally proved the concept recently, is shown that generated voltage is linearly dependent on temperature gradient. Thus, in order to

enhance the harvesting efficiency, this latter should be increased as much as possible. Keeping in mind that our goal is to convert light into electricity, a first step of light to heat generation is needed. Let us now show briefly the components forming the nanofluid and the reason behind their choice.

1.2.1 Choice of solid fraction

The first step is to investigate how we can convert the light into heat efficiently, confining the larger part of this latter in a thin layer of fluid, to enhance the temperature gradient and consequently the photo-electric harvesting efficiency. The light-to-heat enhancement in liquid phase occurring upon addition of nanoparticles is well known since 70s and can reach up to 99% conversion efficiency. Several materials have been intensively investigated, but in the last two decades, attention is given to plasmonic materials, particularly interesting because of their great absorption capabilities in specific energy ranges. Among these materials, gold and silver are the most investigated because of their chemical stability. However, lately has been highlighted that they are not suitable materials for large scale applications, mainly due to their high cost, but also because of their low melting temperature and fast electronic heat dissipation. For this reason, a suitable alternative can be found in alternative plasmonic materials, like transition metal nitrides (TMN). In fact, besides their good properties in terms of heat resistance and chemical stability, they also show plasmonic resonance. In the work of Garnett *et al*. [4] It is shown that the ultrafast electron–phonon coupling prevents fast electronic heat dissipation and low thermal conductivity prolongs the heat confinement. These observations result in a higher temperature reached at basically all the wavelengths used for stimulation and all the geometries, besides the resonance one for which the heating is slightly higher in noble metals. The ultrafast coupling also makes them suitable for electro-chemical applications, since the elementary chemical transition occur at a time scale of 1-100ps. [5] In noble metals the light-to-heat generation requires longer times, in the order of ns, to take place, due to the electronic structure. In fact, the free electron undergo to plasmonic resonance when properly excited and the generated hot carriers decay because of electron-electron scatting. This process lasts hundreds of femto-seconds, up to 10 pico-seconds are needed by the electron to couple with the phonon leading to heat dissipation in 1-10 nano-seconds. In other words, the electron-phonon coupling in gold is 25 to 100 time smaller than the one of metal nitrides. [6] The better photothermal attitude of TMN can also be deduce by observing the complex permittivity since the real part has to do with the propagation of the wave in the 'lossless' medium, while the complex part describes the losses due to the electron scattering and the dipole torque friction. In Fig. 3 this quantity is reported as a function of

the wavelength λ for gold (Au), silver (Ag), copper (Cu), titanium nitride (TiN), zirconium nitride (ZrN) and hafnium nitride (HfN). It should be noticed that the overall higher imaginary part suggests a higher dissipation pointing toward a better absorbance. [7] In fact, the Lambert-Beer expression for absorbance α can adapted to the extinction coefficient according to:

$$\alpha = \frac{4\pi\kappa}{\lambda} \tag{1}$$

where κ is the extinction coefficient.

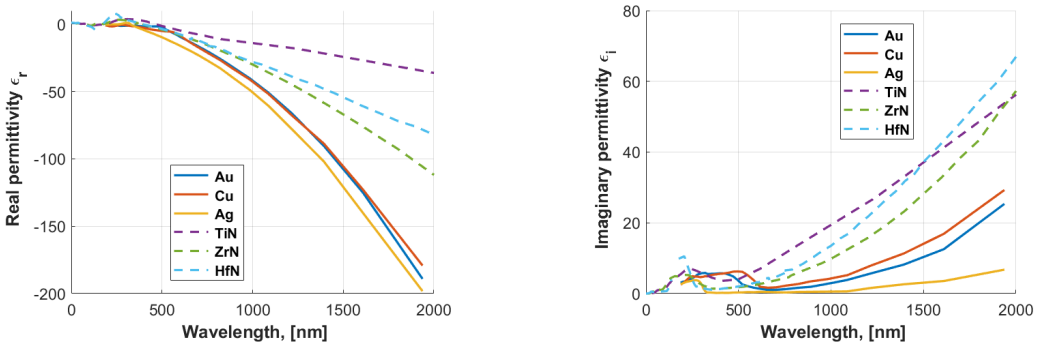

(*a*) (*b*)

Figure 3: *Complex permittivity comparison among metals and TMNs. In 3a is reported the imaginary part and in 3b the real part. Data for metals have been taken from Johnson and Christy [8] while for TMNs from Palik. [9]*

We decided to limit the interest to these three materials, excluding WN or TaN which are forecast to be promising, because of the wide literature provided by the study alternative plasmonic materials. [10] Moreover, it should be noticed that the TMN are not easy to produce because of the material hardness and the difficulty in controlling the structure, morphology, size and defect. [11] The only material that can easily be found in the market in nanopowder form is TiN, while for the HfN and ZrN specialized facilities are needed. For these reasons, we decided to stick with titanium nitride in the next sections of this manuscript. This is provided by PlasmaChem in the form of 20nm particles.

1.2.2 Dimension of the solid fraction

Before the investigation of the possible solvents to be used for the NPs dispersion, we need to get an idea on the range of NPs sizes of interest. To do so, we need to get an idea of the absorption and scattering efficiency these particles have under different circumstances. As a simplification, lets assume to deal with a spherical nanoparticle, common situation in literature, in a highly diluted mixture, so that the

cross-talk among particles can be neglected. These assumptions allow us to use Mie theory to describe the electromagnetic fields inside and outside the particle. This theory is well establish and the detailed derivation is reported elsewhere, [12, 13] but we can summarize the procedure as follow: [11]

- Use spherical coordinates to describe the plane wave. This is actually a tricky step but is needed to simplify the later steps in the derivation of the scattering matrix;
- Expansion of the electromagnetic field inside and outside the particle;
- Reduce these function into series expansion: the coefficients are obtained for the field inside a particle and for the scattering field;
- The coefficients of scattering Q_s and extinction Q_e and absorption efficiencies Q_a, are calculated by integrating the Pointing vector with respect to angle and space variables.

This process ends in an infinite series for the scattering C_s and extinction C_e cross section, namely:

$$C_{sca} = \frac{2\pi}{\kappa^2}\sum_{n=1}^{\infty}(2n+1)(|a_n|^2 + |b_n|^2)$$
$$C_{ext} = \frac{2\pi}{\kappa^2}\sum_{n=1}^{\infty}(2n+1)Re(a_n + b_n)$$

where the coefficients of the series are:

$$a_n = \frac{\mu m^2 j_n(mx)[xj_n(x)]' - \mu_1 j_n(x)[mxj_n(mx)]'}{\mu m^2 j_n(mx)[xh_n^1(x)]' - \mu_1 h_n^1(x)[mxj_n(mx)]'}$$
$$b_n = \frac{\mu_1 j_n(mx)[xj_n(x)]' - \mu j_n(x)[mxj_n(mx)]'}{\mu_1 j_n(mx)[xh_n^1(x)]' - \mu h_n^1(x)[mxj_n(mx)]'}$$

with the prime indicating the derivative w.r.t. the argument in parentheses, m is the ratio among the refractive index n_p of the particle and the medium n_m, x represents the size parameter, i.e. the product of wavevector k and r, the radius of the particle and j_n^1, h_n^1 are the Bessel and Hankel functions of the first kind, respectively.

Implementing this in a MATLAB code, it is possible to estimate the scattering and absorption efficiencies, which are the normalization of the respective cross sections on the geometrical cross section of the particles. Limiting the interest on the range

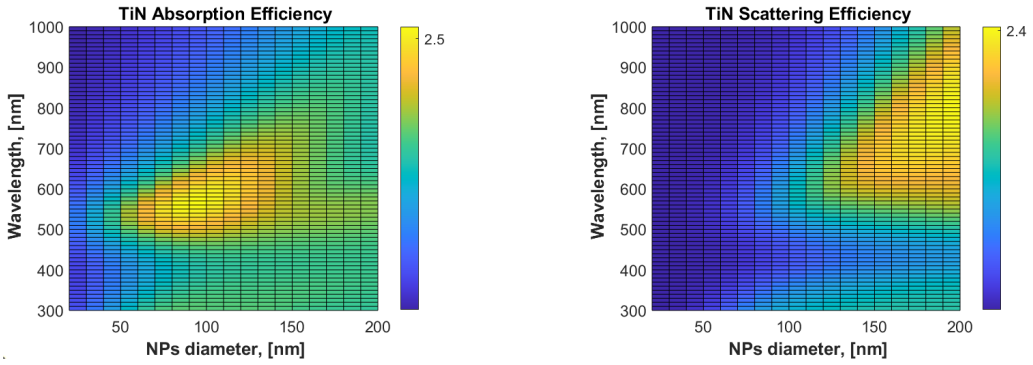

(*a*) (*b*)

Figure 4: *Mathematical model of the photon-NP interaction according to Mie model: 4a absorption and 4b scattering efficiencies of titanium nitride nanoparticles as a function of nanoparticles size and incident photon energy.*

experimentally investigate, i.e visible (Vis $\lambda_{min} = 300$nm) and near infrared (NIR $\lambda_{min} = 1000$nm) range and following the procedure suggested by Baffou [14] reporting on the same graph the scattering and absorption cross section, we obtain information on the threshold in NPs sizes, since the goal is to keep absorption higher than scattering in thermal applications. In order to know what is the wavelength of the incident photon we should investigate, we first need to look into the dependence of $Q_{sca,abs}$ on this latter at fixed diameter. To allow a better visualization of the trend, assuming the particle to be surrounded by water, a 3D plot is reported in Fig.4 for the TiN. Similar treatment can be done for ZrN and HfN showing an absorption peak at $d_{ZrN} = 55$nm and $d_{Hf} = 65$nm. Around $d_{TiN} = 100$nm the particles show a better absorption throughout all the spectrum and a quite limited scattering, giving a first indication about the size. With a fine tuning, it can be shown that the maximum absorption is given by particles with diameter $d = 90$nm. Notice that the maximum scattering under such dimension is given for $\lambda = 650$nm, thus if the particles sizes are lower that the trade value at this λ, absorption will dominate for all the spectra. In Fig.5 these quantities have been reported as functions of the particle sizes.

Interesting is to notice the much larger threshold value for TiN, suggesting a somewhat larger range of absorption. Given these observation, the sizes of the particles will be kept below the critical diameter of $d_{cri} = 100$nm. For sake of completeness, a study on the dependence of sizes should be performed. In Fig.6 are reported the absorption/scattering efficiencies as function of the impinging λ for different NP sizes. The idea would be to investigate three sizes, where we have a situation in which the scattering contribution is negligible, i.e. $d = 20$nm, thanks to the very low particle sizes, an intermediate situation where there are both contribution but

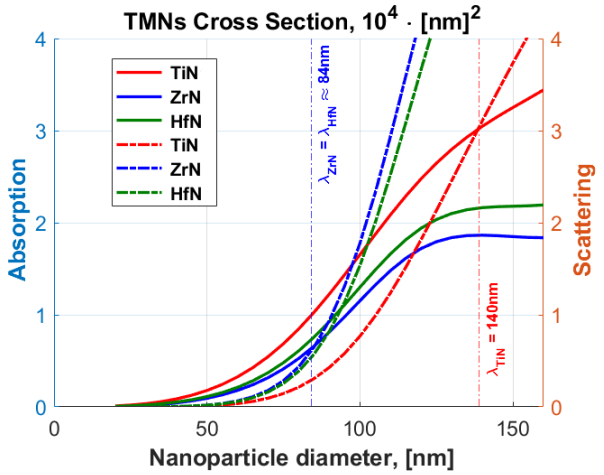

Figure 5: *Trade of in scattering (broken lines) and absorption (full lines) cross section of different TMNs, illuminated by* $\lambda = 650nm$ *and surrounded by water* $n_m = 1.34$

absorption still dominates and a final one, where both take place as a competitive interaction, $d = 100$nm.

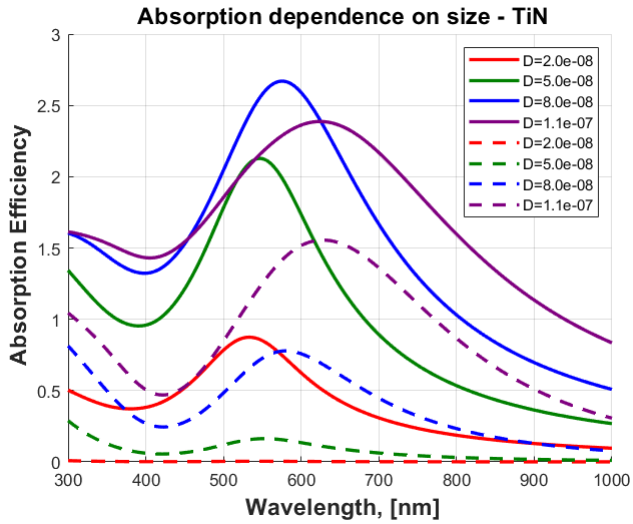

Figure 6: *Absorption (solid) and Scattering (dashed) efficiencies of TiN nanoparticles, given at different sizes, as a function of the incident photon wavelength.*

To be noticed that the performance of the material under radiation are not the only factor in the dimension. The stability of the nanofluid is severely affected by the nanoparticles size, however, it is commonly accepted that under 100nm size, the dispersion of the powders becomes quite easy since the Brownian motion is sufficient to prevent agglomeration. Consequently, also the choice of the solvent plays an important role, given the dipole interaction it can provoke, enhancing the separation. Moreover, the density and viscosity can be tuned to increase the range

of possible particle sizes, even though heat management must be kept into account.

1.2.3 Choice of the Solvent

The dependence of the thermoelectric effect on the temperature gradient leads to investigate methods to improve the heat confinement in a region of the fluid. However, it should be remembered that the thermal conductivity of the fluids is deeply affected by the addition of nanoparticles, resulting in an overall enhancement. So, a tuning on the fluid properties and the nanoparticle concentration is needed. As a first analysis, because of the wide literature produced water-based colloids, [15] de-ionized water is chosen as solvent. It is expected to be a good dispersion mean thanks to the polarity of water molecules and because the materials of interest are not dissolved in water.

For these experiments, the titanium nitride nanopowder is provided by Plasmachem. The TEM picture (Fig. 7a) and dynamic light scattering analysis (Fig. 7b) show that the particles size lie around in the order of 10nm.

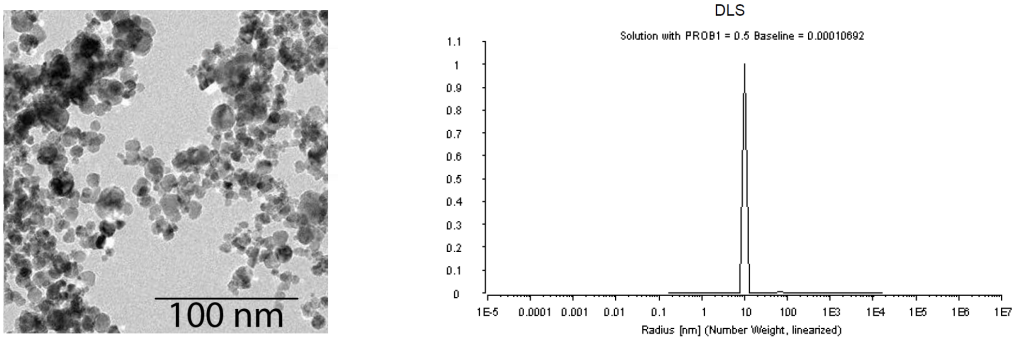

(*a*) (*b*)

Figure 7: *7a Transmission electron microscopy image of titanium nitride nanopowder and 7b dynamic light scattering.*

In order to disperse them, a protocol is followed for all the samples to guarantee uniformity. The mixture of powder and fluid were magnetically stirred at 400rpm for 2h and successively horn sonicated for an hour at 40% amplitude with a cycle of 10s ON and 30s OFF to avoid overheating. The mixture is let cool down for 24 hours and sonicated in bath for 15 min before the experiment. The colloidal suspension has been observed to be stable over long time, in the sense that no supernatant fluid is formed after two weeks of complete rest, but a partial sediment is formed after 2-3 days. However, this is easily re-dispersable with bath sonication. All considered, the solution can be considered uniform and stably dispersed accounting for the relatively short time of the experiments.

Using the first apparatus (see Fig. 1a) and solar simulator light source, the heating throughout the fluid is monitored by means of type k thermocouples and a data acquisition (DAQ) system. For sake of simplicity, we will refer the samples as XX_YY_ZZ where XX represents the solid fraction, TiN in this case, YY is the solvent and ZZ the weight concentration. As an example, the first investigate sample is a 0.5%wt TiN nanoparticles in water, thus it will be referred as TiN_DIW_05. Starting with this, in Fig. 8a the temperature variation is reported in time.

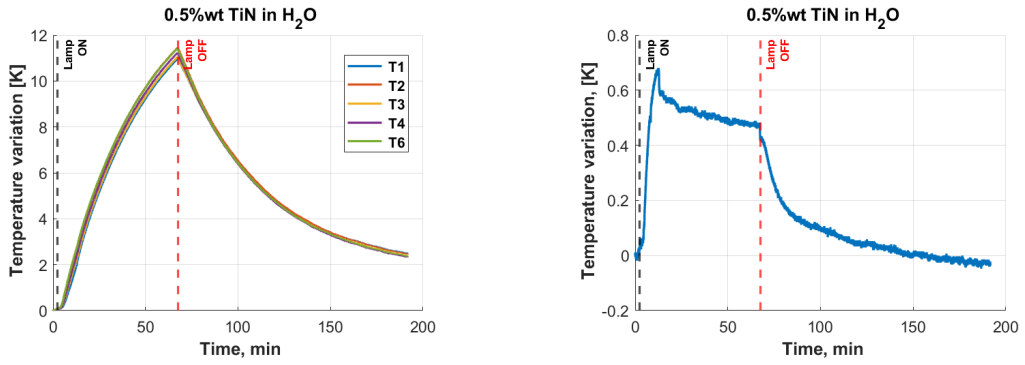

(*a*) (*b*)

Figure 8: *Heating behaviour of the TiN_DIW_05 sample: 8a temperature variation recorded by each thermocouple, 8b temperature difference among the first (T1) and second (T2) thermocouple.*

The increase in temperature is uniform throughout the whole fluid, as evidenced by Fig. 8b where the temperature difference among the first two thermocouple is reported. Moreover, it should be noticed that the heating takes roughly an hour to reach 11K. The uniformity of the heating is mainly due to the low viscosity of the water which is promoting the convection and consequently the heat distribution. Moreover, the high thermal conductivity of the solvent results in a very poor heat confinement, which makes it not suitable for our applications. For this reason, we decided to avoid the test of other solvents like ethanol, 2-propanol, toluene or kerosene, that even though with a much lower thermal conductivity, roughly one forth of the water, have viscosity similar to the water one, without accounting for they low temperature boiling point. Thus, fatty acid or oils [16, 17] represent a better choice, also considering their use as surfactants. Oleic acid (OA) shows a thermal conductivity around $0.15\text{W m}^{-1}\text{K}^{-1}$ [18] and density close to water, making it suitable for nanoparticles dispersion. Moreover, it is typically used to promote the stability of titanium particles. [19] Three samples with 0.1-0.2 and 0.5%wt concentration have been realized following the same dispersion procedure, with the addition of water bath cooling to avoid overheating. After thermalize the mixtures at room temperature, the characterization is repeated. In Fig. 9 is reported the

temperature variation of the thermocouples in TiN_OA_05 for sake of comparison with water case.

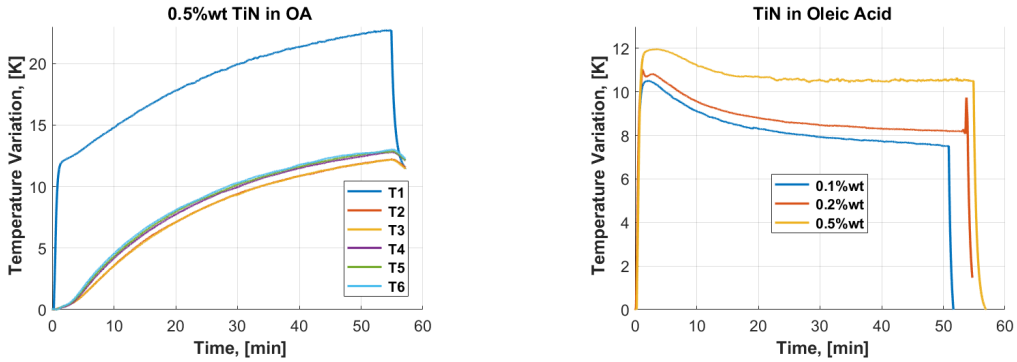

(*a*) (*b*)

Figure 9: *Heating behaviour of the TiN_OA samples: 9a temperature variation recorded by each thermocouple in 0.5%wt sample and 9b temperature difference among the first* $(T1)$ *and second* $(T2)$ *thermocouple for different solid fractions.*

The first thing that should be noticed is the sudden increase of temperature occurring in the first thermocouple placed at 5mm from the illuminated surface. Contrary to the water case, where up to 60 min are needed to reach a temperature variation of 11K, oleic acid takes only $\approx$ 60s to reach the same variation. In Fig. 9a it seems that thermocouple number three reaches a lower temperature compared to the other. This may be due to a lower sensitivity due to a poor contact in the DAQ during the experiments. A more interesting explanation is found by analysing the light source, i.e. the sun spectra, having a large component in the infrared range. It is possible that part of the radiation passes through the fluid to be then absorbed or reflected back by the glass wall on the rear part of the chamber. This provokes heating in the back part of the cell explaining the temperature trend, with minimum in the center. However, as appreciable in Fig. 9b reporting the temperature difference among the first two thermocouples, the largest part of the heat is still confined in the first 5 to 10 mm. This already gives some ideas of the dimension the liquid container should have. Remarkable is also the trend observed with the weight concentration, indicating that at 0.5%wt a stable gradient is reached faster and holds more in time. However, further analysis are needed to reach suitable conclusion and a complete characterization is reported in following sections.

As a final remark, it is interesting to notice the overshoot in temperature occurring in the first 5 minutes. This observation leads to imagine that a suitable operation condition is given under pulsed illumination, rather then a continuous one. This situation is reported in Fig. 10 where fluids are subjected to 50s of illumination and

50s of dark, repeated 4 times consecutively to show repeatability.

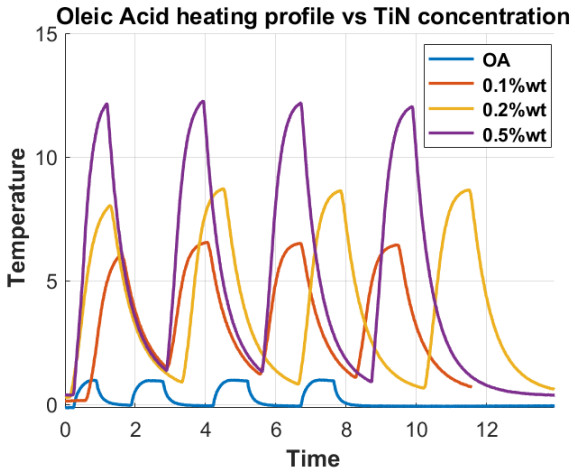

Figure 10: *Temperature difference among thermocouples T1 and T2 in TiN_OA nanofluids at different concentrations.*

The trend with the concentration is repeated, underlying a better heat confinement probably related to the enhanced capability of photon absorption, due to the higher number of particles available. The dephasing among the curve is only due to the non-perfect synchronization of the experiments. Worth to mention is the comparison with the bare oleic acid, which evidence the strong enhancement brought by the solid phase addition.

1.3 Photothermal dependence on the solid fraction

The role of solid fraction in nanofluid thermal conductivity is well investigated, but very few are the experiments dealing with the characterization of the photothermal conversion and heat storage. In this section, the temperature measurement of different weight concentration TiN in oil are reported, and the heating dependence on the radiation wavelength is discussed. It should be noted that previously the sun simulator was used as source, leading to an irradiance of $I_{sun} \approx 1000\ Wm^{-2}$ distributed according so the sun spectra. Here, LEDs are used for two reasons: the tunable irradiance, with dependence on both the distance and the supply voltage, and reduced bandwidth, allowing the investigation of specific excitation. The characterization of irradiance dependencies is carried out by means of a power meter performing a sweep on the voltages ad different distances from light source. To allow more careful control, a digital voltage controller coupled with a user interface is used to stabilize the light source, providing the desired power and waveform. To cover the UV, visible and near infrared (UV-Vis-NIR) part of the spectra, six LEDs are adopted, spectra and their de-convolution in two Gaussian distribution, are reported

in Fig. 11, showing peak wavelengths of $\lambda_p = 375, 420, 530, 625, 780, 940$nm and a waverange of ± 10nm.

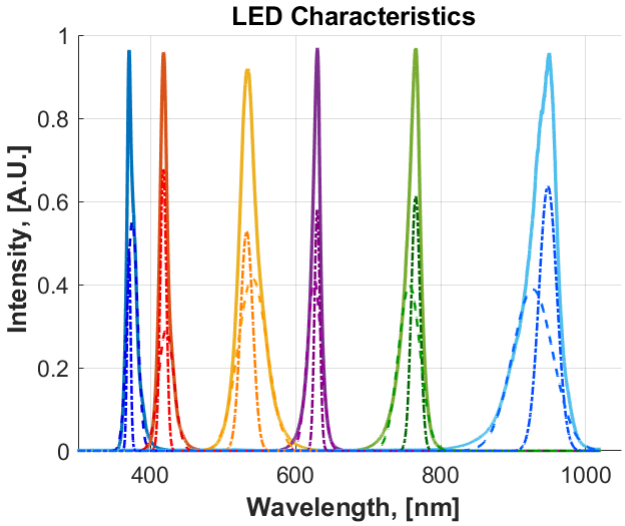

Figure 11: *Spectra of the LEDs used as light source. The dashed and dotted lines represent the first and the second Gaussian distribution, used to reproduce the profiles.*

The fluid prepared for the analysis have weight concentration of $0.03, 0.06, 0.1, 0.3, 0.5$%wt realized using same powder and dispersion procedure described in previous section. The LED irradiance is set to 400W m^{-2} for all λ_p in order to provide the same input energy to the mixture. To be noticed that this will mean a different number of photons which consequently should be accounted in the estimation of photothermal efficiency. The measurements are taken for up to $1h$, until the achievement of a plateau. The discharge profile is also recorded to provide a complete charge (heating) discharge (cooling) loop. For sake of order, the raw measurement of the eight thermocouples temperature trend are not reported since the number of graphs and lines would be overwhelming. A better way to represent the data is provided in Fig. 12 where the surface plot (or thermal maps) show the maximum temperature variation as a function of the fluid depth, meant as the distance from the impinging wall, i.e. the thermocouples spacing, and λ_p. Notice that the maximum temperature is obtained by modeling the system as an RC circuit, to obtain the charge discharge time constants τ, and fitting the hating cooling profiles with the corresponding formulas:

$$T_c(t) = T_{max}\left(1 - \exp^{-\frac{t}{\tau_c}}\right) + T_0$$

$$T_d(t) = T_{max}\exp^{-\frac{t}{\tau_d}} + T_0$$

To improve the comparison among the different samples, the colorbar is set constant to point out at a glance the temperature trend on the concentration. The bare oleic

acid, with no solid phase, is reported to give the reader a baseline.

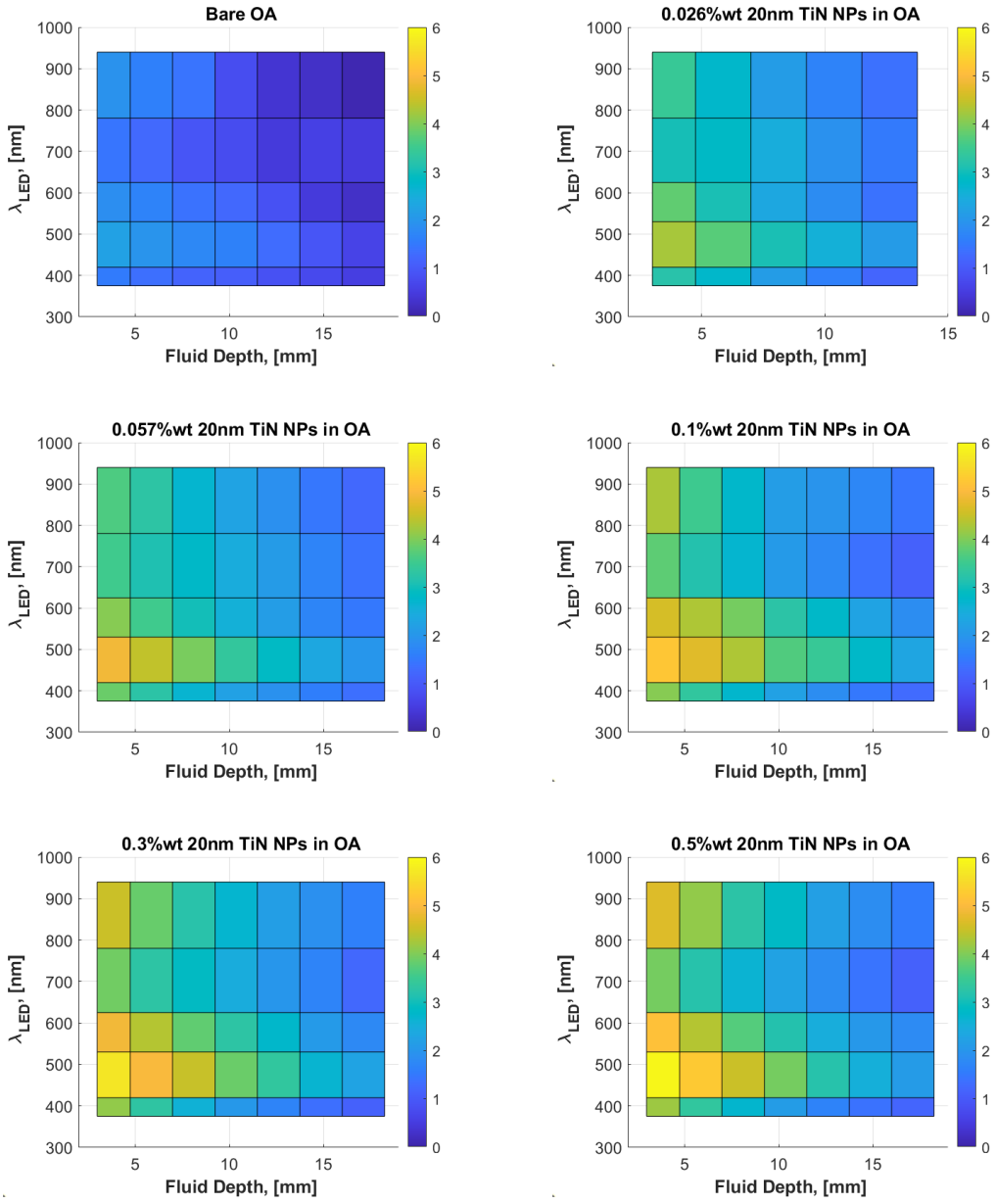

Figure 12: *Thermal maps of the TiN_OA samples at different weight concentration and excitation wavelength.*

To extract the maxima, the function is evaluated at three hours, to ensure the saturation is completely reached. Looking at the color-bars, it can be immediately observed that the concentration is influencing the maximum reachable temperature, even though a saturation trend seems to occur. However, even though representing very conveniently the overall situation, it is difficult to verify these hypotheses. For this reason, in Fig. 13a are reported the temperatures of thermocouple 1, where the

saturation behaviour can be appreciated.

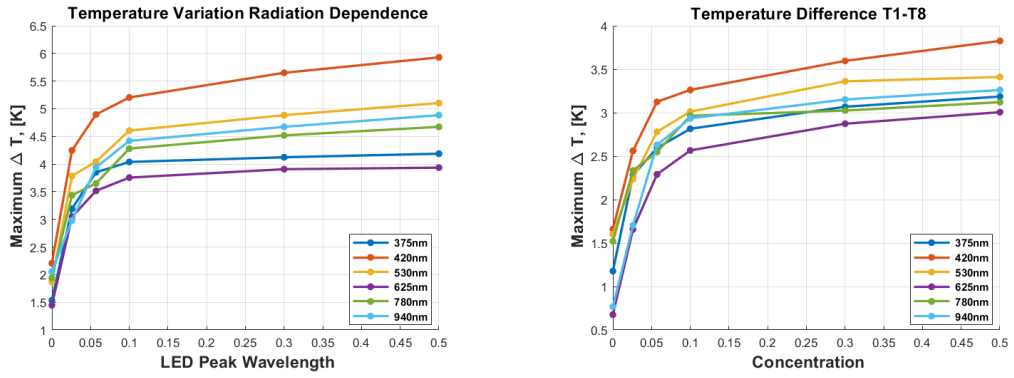

(*a*) (*b*)

Figure 13: *Temperature trend as a function on nanoparticles concentration at different LED λ_p: 13a show the absolute temperature variation of the first thermocouple only, and 13b is the overall temperature gradient recorder among the first (closer) and last (farthest) thermocouples*

In principle, this temperature difference could be related to an offset, meaning that the temperature of the whole fluid is actually increasing. This can be verified by observing the difference among the closer, with respect to light source, and the farthest thermocouple. In fact, if the temperature increase with concentration is constant throughout the fluid, this difference should be kept constant. In Fig. 13b it can be noticed that the same trend is maintained, indicating the increasing heat confinement. Interesting is to notice that the position of green ($\lambda_p = 780$nm) and blue ($\lambda_p = 375$nm) lines is changed in this latter plot. This indicated that the heating occurring at 780nm is penetrating more inside the fluid, giving interesting hints on a possible nanosized liquid light sensor, discerning the impinging light on the penetration depth. It can be noted that the system photothermal efficiency increases noticeably when passing from 0.03%wt to 0.1%wt, to then saturate at higher concentrations for basically all the cases unless the resonance frequency, where the saturation seems to occur for higher concentration. Reporting, just for the first thermocouple, the maximum temperature reached versus the radiation wavelength, we can see a peak at λ_p, see Fig. 14a. This is reasonable if we compare this trend with absorption spectra, see Fig. 14b, which is basically replicating the trend. Interesting is to notice the increase of absorption, upon concentration, in the NIR region probably because multi-scattering processes, which finds basis when observing the sudden increase in conversion efficiency when passing from 0.03%wt to 0.1%wt (Fig. 13).

From the absorption spectra has been remove the baseline using a MATLAB func-

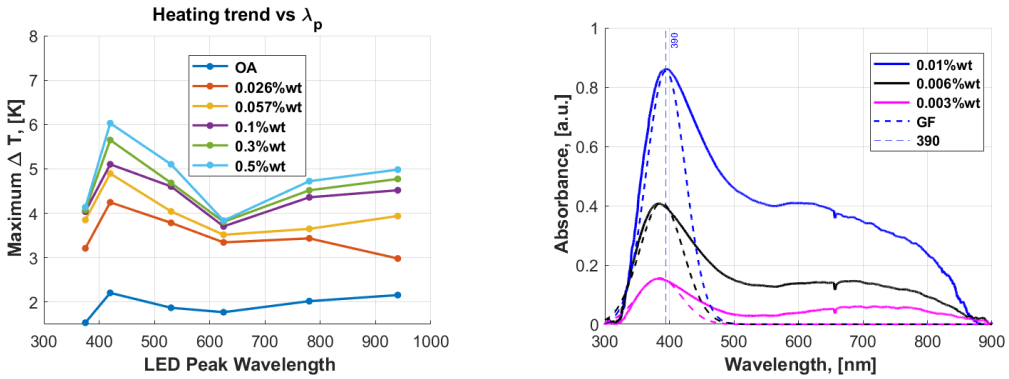

(*a*) (*b*)

Figure 14: *14a Heating behaviour of TiN_OA suspensions using different light sources. 14b Absorbance spectra at different concentration. The Gauss fit identifies the resonance frequency.*

tion and the Gauss fit are used to determine the resonance wavelength. Notice that increasing the concentration, there is a common phenomena occurring, i.e. a red shift, indicating that at higher concentration probably the resonance will go toward $\lambda = 400$nm or more. Finally, The trend of temperature as a function of distance from the light source, is reported in Fig. 15, where an exponential decay is observed according to the expectations. In fact, the low thermal conductivity of the solvent and its high kinematic viscosity preventing the convection, limit greatly the extension of the heated layer. This gives indication of how the chamber should be designed to guarantee a sufficient gradient. Notice that the temperature increase with the concentration is generally followed by a slight increase in the temperature of the farther fluid layer. This is probably connected to the thermal conductivity enhancement provoked by the solid phase, but further analysis are needed since now always is possible to identify a clear trend. Discussion on the penetration depth of the radiation are not possible at present because the spacing among thermocouples is to high to allow good resolution. Moreover, it would be interesting to 3D map the temperature of the fluid for a complete treatment. However, there seems to be no tool allowing to measure in immersion mode the temperature punctually on a surface. In the future works, we can either use flat thermristor, which at least provide an enhanced average due to their area, or shrink down the chamber area.

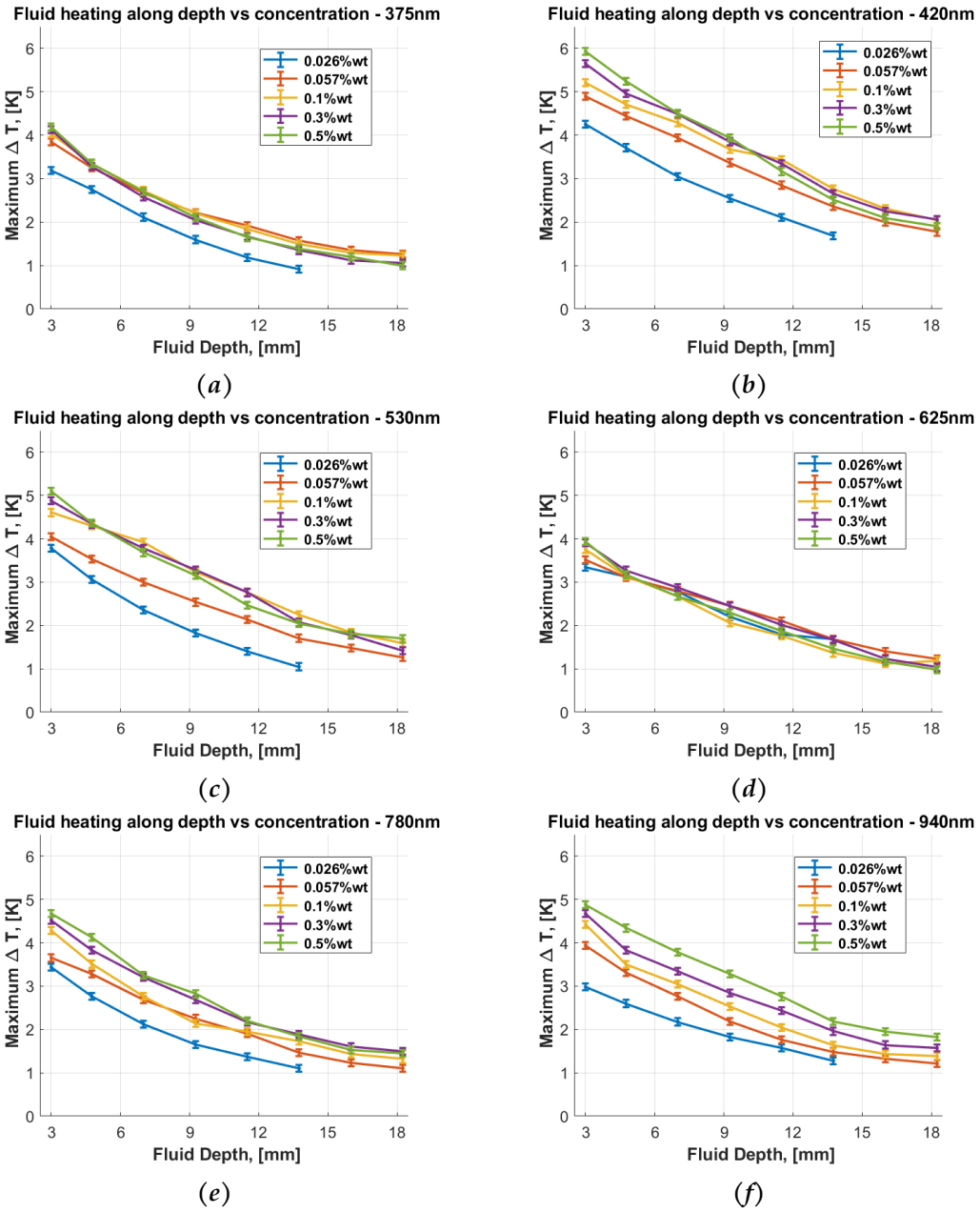

Figure 15: *Temperature trend inside the colloidal mixture. Each graph represents the situation under different radiation.*

2 System Efficiency

In this section, we want to conclude the work by calculating the photothermal efficiency of the system and observe the trend with concentration of TiN in oleic acid. For these experiments, we have used an irradiance of $I = 40 mW cm^{-2}$ and, according to the work done by Luo *et al.* [20] on the temperature increase in oil-based nanofluid at different radiation intensities, the temperature increase obtained is in line with Al_2O_3, SiO_2, C and Ag nanofluids. However, this is not true for other experiments [21] where an increase of around 20°C is observed. This discrepancy must be related to the different radiation intensity ($\approx 700 \mathrm{Wm}^{-2}$ as well as the different excitation spectra used, i.e. solar spectra. Isolation of the system is also playing an important role and it must be kept in memory that the system as such does was not isolated, with the upper part of the fluid being exposed to air.

To estimate the photothermal efficiency of the experimental setup under analysis, we address the attention first to the estimation of the energy stored in the fluid. In literature, it is commonly accepted that, in case of nanofluid flowing under an impinging radiation, the variation of internal energy can be expressed as:

$$\Delta U = \dot{m} c_p (T_{out} - T_{in})$$

with $\dot{m}$ indicating mass flow rate and T_{out}, T_{in} the outlet and inlet temperatures. The specific heat capacity c_p depends on the fluid temperature according to the relation: [22]

$$\begin{aligned} c_p^{18} &= 2.172 + 0.0022 \cdot (T - 80) \\ c_p^{*} &= c_p^{18} + 0.0104 \cdot (C - 18) \\ c_p &= c_p^{*} - 0.0566 \cdot U \end{aligned}$$

where c_p^{18} is the specific heat at the average carbon number C while c_p^* is the one considering one double bond U. The slightly different experimental situation introduces the change of fluid temperature in time, which should be considered to correctly estimate the efficiency, rather then considering an average stationary temperature. Thus, the internal energy variation in the system is given by

$$dU = C_V \, dT + \left[T \left(\frac{\partial P}{\partial T} \right)_V - P \right] dV \longrightarrow \Delta U = \rho \int dV \int c_v(T) \, (T(t) - T_0) dt$$

Where the pressure P and the volume V are considered constant in this system, as well as the density ρ thanks to the uniformity and homogeneity of the nanofluid.

Thus, we can further simplify in:

$$\Delta U = \rho V_t \int_0^t c_v(T)\,(T(t) - T_0)dt$$

The relation between temperature and time is obtained by modeling the experimental system as a RC circuit as reported in *Photothermal dependence on the solid fraction* section and T_0 is set to zero by subtracting the initial fluid temperature. Finally, the photothermal efficiency of the system is given, accordingly to the definition, by the ratio of the energy stored in the system ΔU and the energy provided in input, i.e. $E_i = I \cdot A \cdot t$ with I irradiance, A cross sectional area shined and t time. The results are reported in Fig. 16, where the error is calculated according to the propagation error, derivative method.

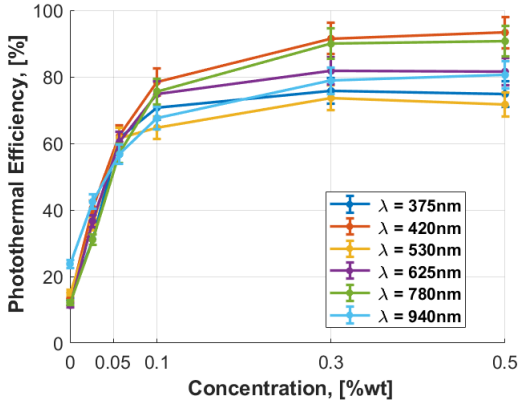

Figure 16: *Oleic acid based titanium nitride nanofluid photothermal efficiency dependence on weight concentration of the solid phase under different irradiation waves.*

The profile faithfully follows the trend of temperatures, with some slight change on λ_p due to the different times of acquisition. Furthermore, already at $0.026\%wt$ the photothermal efficiency is enhanced of $\approx 100\%$, underlying the importance of the solid phase. These results are in line with the few available literature, if the radiation intensity and the different light source are taken properly into account. [20, 23, 24] It is important to underline that it is fundamental to account for the temperature time dependency when there is no fluid flow. The maximum photothermal efficiency is given for the photon having energy closer to the plasmon frequency of the particles, i.e. $\lambda_p = 420$nm. The maximum value of 93% efficiency is reached at this frequency for the $0.5\%wt$ sample, corresponding to an overall enhancement of 700% with respect to the bare oleic acid. This promising results open the path toward investigation of photo-to-thermoelectric applications.

References

[1] Olena Okhay and Alexander Tkach. Impact of Graphene or Reduced Graphene Oxide on Performance of Thermoelectric Composites. *C*, 7(2):37, 2021.

[2] Sanjay Kumar, Nikhil Chander, Varun Kumar Gupta, and Rajeev Kukreja. Progress, challenges and future prospects of plasmonic nanofluid based direct absorption solar collectors – a state-of-the-art review. *Solar Energy*, 227:365–425, October 2021.

[3] K Anu and J Hemalatha. Magnetically tuned thermoelectric behavior of Zn-doped magnetite nanofluids. *Nanotechnology*, 32(2):025707, 2020.

[4] Sven H. C. Askes and Erik C. Garnett. Ultrafast Thermal Imprinting of Plasmonic Hotspots. *Advanced Materials*, 33(49):2105192, 2021.

[5] Devin B. O'Neill, Sean K. Frehan, Kaijian Zhu, Erwin Zoethout, Guido Mul, Erik C. Garnett, Annemarie Huijser, and Sven H. C. Askes. Ultrafast Photoinduced Heat Generation by Plasmonic HfN Nanoparticles. *Advanced Optical Materials*, 9(19):2100510, 2021.

[6] Benjamin T. Diroll, Soham Saha, Vladimir M. Shalaev, Alexandra Boltasseva, and Richard D. Schaller. Broadband Ultrafast Dynamics of Refractory Metals: TiN and ZrN. *Advanced Optical Materials*, 8(19):2000652, 2020.

[7] University of Reading. Absorption and extinction coefficient theory, 2017.

[8] P. B. Johnson and R. W. Christy. Optical Constants of the Noble Metals. *Physical Review B*, 6(12):4370–4379, 1972.

[9] Edward Palik. *Handbook of Optical Constants of Solids*. Amsterdam University Press, Amsterdam, Netherlands, 1998.

[10] Adrien Lalisse, Gilles Tessier, Jérome Plain, and Guillaume Baffou. Plasmonic efficiencies of nanoparticles made of metal nitrides (TiN, ZrN) compared with gold. *Scientific Reports*, 6(1), 2016.

[11] Yin Ma, Lijun Xiong, Yao Lu, Wenqiang Zhu, Haihong Zhao, Yahui Yang, Liqiu Mao, and Lishan Yang. Advanced Inorganic Nitride Nanomaterials for Renewable Energy: A Mini Review of Synthesis Methods. *Frontiers in Chemistry*, 9, 2021.

[12] Craig F. Bohren and Donald R. Huffman. Absorption and Scattering of Light by Small Particles. *1998 WILEY-VCH Verlag GmbH Co. KGaA*, 1998.

[13] Diran Deirmendjian. *Electromagnetic Scattering on Spherical Polydispersions*. RAND Corporation, Santa Monica, CA, 1969.

[14] Guillaume Baffou. Thermoplasmonics. *Thermoplasmonics Heating Metal Nanoparticles Using Light*, 2017.

[15] Satoshi Ishii, Ramu Pasupathi Sugavaneshwar, and Tadaaki Nagao. Titanium Nitride Nanoparticles as Plasmonic Solar Heat Transducers. *The Journal of Physical Chemistry C*, 120(4):2343–2348, 2016.

[16] Amir Al-Ahmed, Ahmet Sarı, Mohammad Abu Jafar Mazumder, Billel Salhi, Gökhan Hekimoğlu, Fahad A. Al-Sulaiman, and Inamuddin. Thermal energy storage and thermal conductivity properties of fatty acid/fatty acid-grafted-CNTs and fatty acid/CNTs as novel composite phase change materials. *Scientific Reports*, 10(1), 2020.

[17] Carolina Cárdenas-Ramírez, Maryory A. Gómez, Franklin Jaramillo, Angel G. Fernández, and Luisa F. Cabeza. Experimental determination of thermal conductivity of fatty acid binary mixtures and their shape-stabilized composites. *Renewable Energy*, 175:1167–1173, 2021.

[18] Ramanujam Lenin and Pattayil Alias Joy. Role of base fluid on the thermal conductivity of oleic acid coated magnetite nanofluids. *Colloids and Surfaces A: Physicochemical and Engineering Aspects*, 529:922–929, 2017.

[19] Rezvan Ghasemi, Alireza Fazlali, and Amir H. Mohammadi. Effects of TiO2 nanoparticles and oleic acid surfactant on the rheological behavior of engine lubricant oil. *Journal of Molecular Liquids*, 268:925–930, 2018.

[20] Zhongyang Luo, Cheng Wang, Wei Wei, Gang Xiao, and Mingjiang Ni. Performance improvement of a nanofluid solar collector based on direct absorption collection (DAC) concepts. *International Journal of Heat and Mass Transfer*, 75:262–271, 2014.

[21] Haichuan Jin, Guiping Lin, Lizhan Bai, Muhammad Amjad, Enio Pedone Bandarra Filho, and Dongsheng Wen. Photothermal conversion efficiency of nanofluids: An experimental and numerical study. *Solar Energy*, 139:278–289, 2016.

[22] Xiaoyi Zhu. Prediction of specific heat capacity of food lipids and foods, 2015.

[23] Sujit Kumar Verma and Arun Kumar Tiwari. Progress of nanofluid application in solar collectors: A review. *Energy Conversion and Management*, 100:324–346, 2015.

[24] Changhui Liu, Yu Qiao, Peixing Du, Jiahao Zhang, Jiateng Zhao, Chenzhen Liu, Yutao Huo, Cong Qi, Zhonghao Rao, and Yuying Yan. Recent advances of nanofluids in micro/nano scale energy transportation. *Renewable and Sustainable Energy Reviews*, 149:111346, 2021.